A Collision-resilient Flying Robot

• •

Adrien Briod and Przemyslaw Kornatowski
Laboratory of Intelligent Systems, École Polytechnique Fédérale de Lausanne, 1015 Lausanne, Switzerland
e-mail: Adrien.Briod@epfl.ch, Przemyslaw.Kornatowski@epfl.ch
Jean-Christophe Zufferey
senseFly SA, 1024 Ecublens, Switzerland
e-mail: Jean-Christophe.Zufferey@sensefly.com
Dario Floreano
Laboratory of Intelligent Systems, École Polytechnique Fédérale de Lausanne, 1015 Lausanne, Switzerland
e-mail: Dario.Floreano@epfl.ch

Flying robots that can locomote efficiently in GPS-denied cluttered environments have many applications, such as in search and rescue scenarios. However, dealing with the high amount of obstacles inherent to such environments is a major challenge for flying vehicles. Conventional flying platforms cannot afford to collide with obstacles, as the disturbance from the impact may provoke a crash to the ground, especially when friction forces generate torques affecting the attitude of the platform. We propose a concept of resilient flying robots capable of colliding into obstacles without compromising their flight stability. Such platforms present great advantages over existing robots as they are capable of robust flight in cluttered environments without the need for complex sense and avoid strategies or three-dimensional mapping of the environment. We propose a design comprising an inner frame equipped with conventional propulsion and stabilization systems enclosed in a protective cage that can rotate passively thanks to a three-axis gimbal system, which reduces the impact of friction forces on the attitude of the inner frame. After addressing important design considerations thanks to a collision model and validation experiments, we present a proof-of-concept platform, named GimBall, capable of flying in various cluttered environments. Field experiments demonstrate the robot's ability to fly fully autonomously through a forest while experiencing multiple collisions. © 2013 Wiley Periodicals, Inc.

1. INTRODUCTION

Using robots instead of risking human lives for exploration missions in dangerous environments, such as after earthquakes, fires, or explosions, has many benefits. Flying robots have many advantages as they provide an elevated point of view and can navigate above rubble more efficiently than ground-based robots. However, cluttered environments such as collapsed buildings, caves, or forests all present great challenges for flying platforms because of the high number of obstacles, the absence of GPS, the unstructured nature of the environment, and the poor visual conditions.

Existing obstacle-avoidance techniques based on vision sensors (Zufferey, Beyeler, and Floreano, 2009) or distance sensors (Roberts, Stirling, Zufferey, and Floreano, 2007; Schafroth, Bouabdallah, Bermes, and Siegwart, 2008) have some success in fairly simple and structured environments. More advanced techniques use simultaneous localization and mapping (SLAM) algorithms and allow flying robots to navigate around obstacles in complex unknown environ-

ments (Bachrach, He, and Roy, 2009; Scaramuzza et al., 2013; Shen, Michael, and Kumar, 2011).

However, there are always situations in which the clutter is too dense, the visual conditions are too poor, or the obstacles are too complex to detect, making collisions unavoidable. Even nature's most agile flyers, such as insects, are not able to avoid all collisions, and are often seen colliding into windows, low-contrast walls, or moving obstacles. While insects recover quickly in the air and continue flying after a collision (Briod, 2008), most flying robots are unable to recover from the disturbance provoked by an impact and are often out of commission after a single collision.

Collision-resilient flying robots are aimed at improving the robustness and locomotion efficiency of existing platforms and addressing the situations in which collisions are unavoidable. These platforms can sustain collisions and remain stable in the air after impacts, which brings many benefits. For example, since collisions are acceptable, such platforms can locomote efficiently through cluttered environments without the caution and low speed often required for sense and avoid approaches. Obstacles do not need to be perfectly (or even partially) detected, which reduces drastically the complexity and weight of the embedded sensors

Direct correspondence to: Adrien Briod, e-mail: Adrien.Briod@epfl.ch

required for navigation. Finally, such robots are more robust to unexpected situations, such as moving obstacles or sensor failures.

Platforms equipped with frames that protect sensitive elements like sensors and propellers from impacts have recently been described (Bristeau, Callou, Vissière, and Petit, 2011). Some protective structures double as locomotion mechanisms on the ground thanks to a passive degree of freedom (Itasse, Moschetta, Ameho, and Carr, 2011; Kalantari and Spenko, 2013). These protective structures are useful when only the yaw axis is affected by a collision, because if an appropriate control strategy is selected (e.g., by leaving the yaw axis uncontrolled during a collision), the stability of the vehicle is not disturbed. However, some impacts can affect the roll and pitch axes of flying platforms, which may cause a fall to the ground because the propulsion system generates accelerations toward undesired directions and may not be able to generate lift. This problem led to the design of protective structures able to withstand falls from a few meters (Klaptocz, Briod, Daler, Zufferey, and Floreano, 2013) as well as uprighting mechanisms, for example passive (Dees and Yan, 2012; Klaptocz, Boutinard-Rouelle, Briod, Zufferey, and Floreano, 2010; Spletzer, Fischer, and Martinez, 2001) or active (Klaptocz, Daler, Briod, Zufferey, and Floreano, 2012). Autonomous flights through a narrow corridor or in a dark room were even demonstrated by such a collision-robust platform (Klaptocz, 2012). However, repeated falls to the ground reduce the distance covered over time and increase energy requirements.

To the authors' knowledge, there is no method that prevents impacts from disturbing a platform's stability in all situations and thus prevents a fall to the ground after a collision. The present paper introduces a method for significantly reducing the disturbances caused by contact with an external object, allowing a new type of resilient flying robot to collide with obstacles while remaining stable. Section 2 presents a collision model and suggests a first set of guidelines for the design of collision-resilient flying robots. Section 3 introduces a mechanical concept for a collision-resilient flying platform, and Section 4 presents a prototype, named GimBall, that has been constructed following this concept. In Section 5, multiple collision experiments are carried out with the prototype in order to validate the model of Section 2 and the concept of Section 3. Additional guidelines are suggested in light of the results obtained from these experiments. Finally, experiments that demonstrate the viability of the concept are presented and show the GimBall robot flying in various cluttered environments while experiencing multiple collisions, including autonomous flights through a forest.

2. COLLISION MODEL

Very little can be found in the literature about the analysis of collisions of aerial vehicles with static objects; the closest
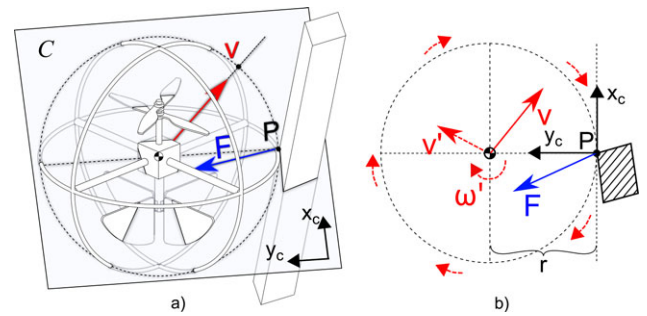
Figure 1. (a) Sample aerial vehicle equipped with a protective frame rigidly attached to the control and propulsion system colliding into a beam. The protective frame is pictured as describing a sphere but could be of any shape. The collision plane C is defined as containing the contact point P, the initial velocity vector $\mathbf{v}$, and the center of mass (COM). (b) Two-dimensional (2D) representation of the aerial vehicle on the collision plane. The velocity $\mathbf{v}'$ just after the impact is contained in C and the rotational velocity ω' just after the collision is normal to C.

topic is the study of flying robots that are in constant contact with rigid surfaces (Marconi and Naldi, 2012). This section focuses on the development of a simple collision model, useful to derive design considerations for better platform stabilization after collisions or to analyze the effect of scale. A formalization of the collisions is also useful in shaping a methodology for testing the performance of disturbance-reduction methods. The main goal of the model is to describe how the aerial vehicle's linear and angular speeds are affected by an impact. A model developed in Cross (2002), improving on the work of Garwin (1969), describes the collisions of a semielastic ball with various types of surfaces, and can be adapted to the case of aerial vehicles after making a few assumptions.

The goal is to study the transformation of the linear velocity just before the impact into an angular speed and a new velocity just after the impact. For the sake of simplicity, the case of a null angular speed just before the impact is considered. It is assumed that there is only one contact point between the aerial vehicle and the obstacle. Also, it is assumed that no significant force other than the contact force is applied on the aerial vehicle during the impact. In other words, the linear and angular accelerations generated by the propulsion and stabilization systems during the collision are considered to be negligible compared to the impact force.

According to Domenech (2005), the collision can be studied in two dimensions on the collision plane C if the angular velocity before the impact is null. As shown in Figure 1, the collision plane C is defined as containing the contact point P, the initial velocity vector $\mathbf{v}$, and the center of mass (COM). C also contains $\mathbf{F}$, the average force applied by the external object on the aerial vehicle during the

impact, as well as $\mathbf{v}'$, the velocity just after the impact. The rotational velocity ω' just after the collision is normal to C. A coordinate system comprised in C is defined with the origin at the contact point P and the Y axis pointing toward the COM. The X axis is called the tangential or horizontal axis, and the Y axis the perpendicular or vertical axis.

A collision of an aerial vehicle with an obstacle can have very different outcomes, depending on the elasticity of the protective structure of the vehicle, the mechanical interlocking or friction with the obstacle, and the rigidity of the obstacle. Typically, the aerial vehicle will bounce away from the obstacle to some extent depending on the elasticity of the protective structure and the rigidity of the obstacle. Also, if the initial velocity is not pointing toward the point of impact and the contact is not frictionless, the collision force will generate torques and thus cause the vehicle to spin. While the dynamics of the interaction occurring during the impact are quite complicated and involve slipping, gripping, or bouncing, the details can be ignored thanks to the introduction of two coefficients of restitution (COR), e_x and e_y (Cross, 2002):

$$e_y = -\frac{v'_y}{v_y}, \tag{1}$$

$$e_x = -\frac{v'_x - r\omega'}{v_x}. \tag{2}$$

The perpendicular COR e_y can vary between 0 and 1 and describes the amount of elasticity in the protective structure and external obstacle. If e_y is equal to 1, the collision is fully elastic and the aerial vehicle will bounce off the obstacle with a reversed sign for the perpendicular speed, while if e_y is equal to 0, the aerial vehicle will stay against the obstacle. The tangential COR e_x can vary between -1 and 1 and describes the amount of friction between the protective structure and the external obstacle, as well as some elasticity, and allows the determination of how much spin is given to the aerial vehicle. If e_x is equal to -1, it simulates a frictionless contact that does not generate any spin. If e_x is equal to 0, it simulates a contact where the aerial vehicle grips the surfaces and the contact point comes to a rest, thus provoking a spin $\omega' = \frac{v'_y}{r}$. If e_x is equal to 1, the contact point bounces back with opposite speed, which provokes an even larger spin. While these coefficients vary from situation to situation, they facilitate a generic approach as they provide scaleless criteria useful to compare the reaction to collisions in different situations or for different platforms. The velocity just after the impact, $\mathbf{v}'$, the angular speed just after the impact, ω', and the average contact force during the impact, $\mathbf{F}$, can then be obtained knowing the velocity $\mathbf{v}$ just before the impact thanks to the conservation of momentum:

$$\omega' = v_x \frac{1}{r} \frac{(e_x + 1)}{\alpha + 1}, \tag{3}$$

$$v'_x = v_x \frac{1 - \alpha e_x}{\alpha + 1}, \tag{4}$$

$$v'_y = -e_y v_y, \tag{5}$$

$$F_x = -\frac{m v_x}{\Delta t} \frac{\alpha}{\alpha + 1}(e_x + 1), \tag{6}$$

$$F_y = -\frac{m v_y}{\Delta t}(e_y + 1), \tag{7}$$

where $\alpha = \frac{I}{mr^2}$ is a scaleless parameter that describes the mass distribution of the aerial vehicle. I is the moment of inertia of the aerial vehicle about the axis normal to the collision plane at the center of mass, m is the mass of the aerial vehicle, r is the distance between the contact point P and the center of mass, and Δt is the duration of the impact, which depends on the stiffness of both the platform and the obstacle.

The velocity after the impact, $\mathbf{v}'$, given by Eqs. (4) and (5), highlights a disturbance in the aerial vehicle's trajectory, provoked by the contact force $\mathbf{F}$ [Eqs. (6) and (7)]. While the velocity direction is affected by the impact (the perpendicular component of the velocity is inversed during the collision), the velocity amplitude after the impact is, however, always less than or equal to the velocity before the impact, which means that the contact forces applied at the COM do not cause the platform to fly at unsafe speeds.

The angular speed after the impact ω' given by Eq. (3) is provoked by the friction force F_x (6), and it describes how the platform is rotating after the impact. It may take significant time for the stabilization system to generate the torques to bring back the angular speed to zero and the attitude of the platform to a stable orientation. This rotation is thus a big issue for conventional platforms whose propulsion systems are rigidly attached to the protective frame, because during the amount of time it takes for the robot to stabilize, the propulsion system creates a force that is not primarily pointing upward. The aerial vehicle may thus quickly lose lift, or gain speed toward the direction in which the propulsion system creates a force.

While smaller aircrafts are more agile according to scaling laws (Kumar and Michael, 2012) and may be able to recover faster from perturbations, it should be noted that smaller aerial vehicles are also more disturbed by collisions. Indeed, ω' scales inversely proportionally to r, which means that for similar aerial vehicles of different sizes colliding at the same speed with an external object, the rotation speed after a collision is larger for smaller aerial vehicles.

To design collision-resilient flying robots of all sizes, the angular speed after a collision needs to be reduced. One first guideline is to fly slowly, as ω' is directly proportional to v_x. Increasing α, the moment of inertia for a given mass and size, may help to reduce ω', but this is not recommended as it will on the other hand affect the stabilization's response time. It is possible to optimize the geometry of the platform
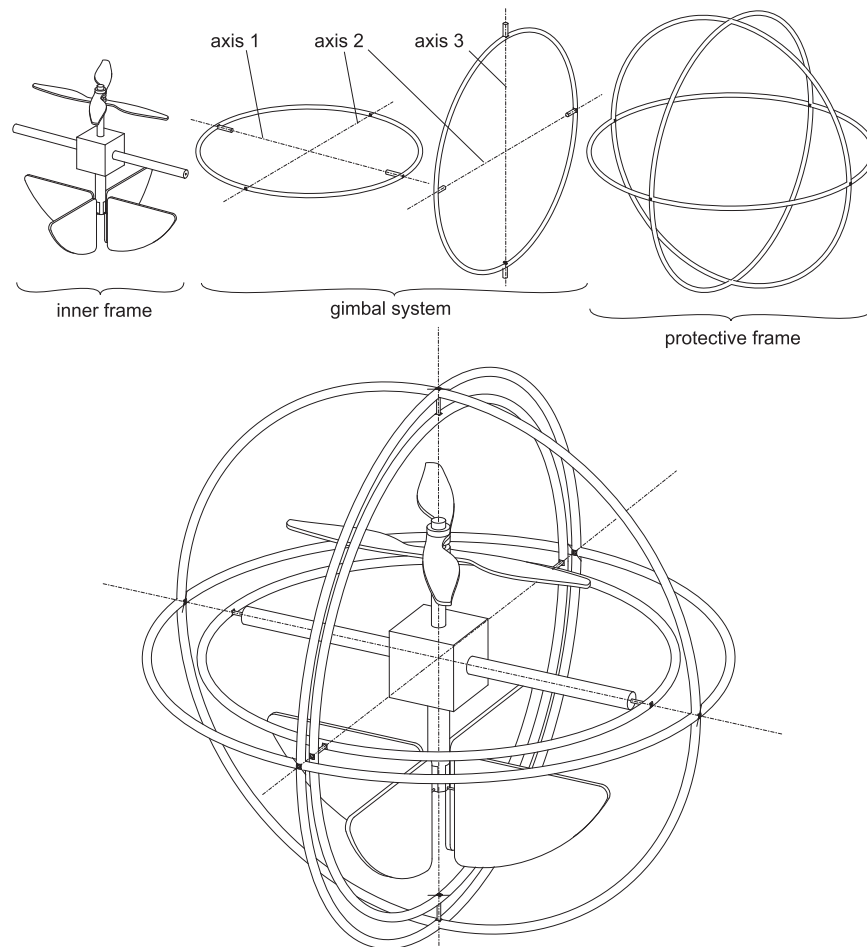
Figure 2. Concept of resilient flying robot comprising an inner frame, a gimbal system, and a protective frame. The inner frame comprises the propulsion and control systems and is assembled inside two gimbals, around which the protective frame is mounted. The outer frame can rotate passively and freely around the inner frame around each of the three rotation axes, which allows the platform to collide with obstacles without directly affecting the orientation of the inner frame.

so as to minimize r when flying toward certain directions, and thus minimize ω'. For example, a very flat platform only flying in the horizontal plane will only get little disturbances on the roll and pitch axes during collisions. However, this is not applicable when flying in all directions, and only lowering the tangential COR e_x remains as a solution. In fact, in the case of frictionless collision ($e_x = -1$), the rotational speed just after the impact is zero, as well as the friction force F_x. Ideally, a protective cage could be made extremely smooth and slippery. Instead of gripping obstacles, it would slide on them, thus never provoking any friction force or rotation of the frame.

3. GIMBAL SYSTEM FOR COLLISION RESILIENCE

To improve the resilience to collisions, the friction force between a protective frame and obstacles should be min-

imized. This is, however, very hard to achieve because protective frames cannot be designed to be perfectly smooth and prevent friction with all obstacles.

The solution introduced in this paper is to mechanically decouple a protective frame from an inner frame by means of a gimbal system, so that the protective frame can passively rotate around the inner frame. The inner frame contains the conventional propulsion and stabilization systems that keep the aerial vehicle aloft by generating an upward force and rejecting small disturbances. The protective frame is directly in contact with obstacles during a collision, and is subject to friction forces that may provoke its rotation. Because the protective frame rotates independently from the inner frame, the friction force does not affect directly the orientation of the inner frame. A design example of the proposed solution is pictured in Figure 2.
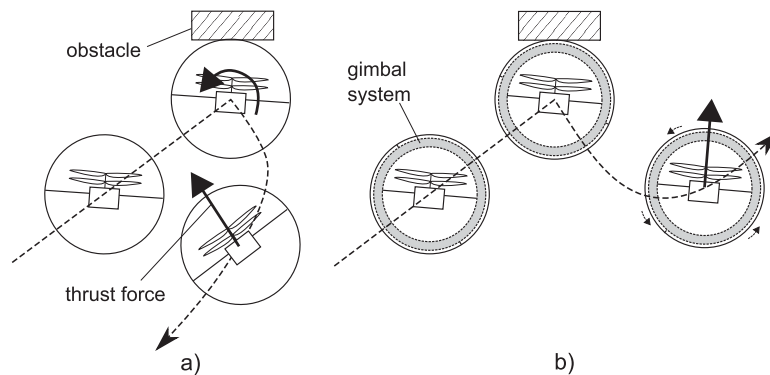
Figure 3. Side view of two situations illustrating the advantages of a resilient flying robot equipped with a gimbal system. While this example is in two dimensions, the concept is the same in three dimensions for contacts anywhere on the outer frame. (a) Example trajectory of a caged aerial vehicle that is strongly disturbed by a collision because the friction force rotates the platform in an unstable orientation. The aerial vehicle thus loses lift and goes in the direction toward which the propulsion system is generating a force. (b) Collision with an obstacle of an aerial vehicle equipped with a gimbal system decoupling the rotation of the outer frame from the inner frame. In this case, the friction force only affects the orientation of the protective frame, and the propulsion system that is contained in the inner frame remains in a stable orientation. The aerial vehicle is only slightly diverted from its original trajectory and can continue toward the intended direction.

Figure 3 illustrates the advantages of the proposed solution over existing caged robots. By minimizing the friction force that is applied on the inner frame during a collision, the platform can remain stable in the air after an impact and continue flying toward its goal. By decoupling the inner frame from the protective frame, the gimbal system also increases the reactivity of the inner frame (and thus its capability to recover from a disturbance) as its moment of inertia is much lower than if the protective frame had been rigidly attached.

To minimize the disturbances affecting the inner frame, several considerations have to be made on the design of the inner frame, the gimbal system, and the protective frame. A first point is to prevent the rotation of the outer frame from being transmitted to the inner frame. Six rotation joints separate the inner frame from the outer frame, and the friction in these joints should thus be minimized, even when they experience important axial loads during a collision. The alignment of the pair of joints used for each axis of rotation is also important to keep the friction low, which advocates for stiff support structures for these joints. Another important consideration is the position of the center of mass.

While it decouples the inner frame from the torques created by the friction force, the gimbal system may be the source of new disturbances. Typically, the external forces applied to the protective frame are applied to each gimbal and the inner frame through the rotation axes, which implies that if the inner frame's COM is not aligned with the rotation axes, a torque is generated on the inner frame. To illustrate this problem, Figure 4 shows a side view of an aerial vehicle equipped with a gimbal system colliding with an obstacle. The COM is misaligned with respect to the intersection of
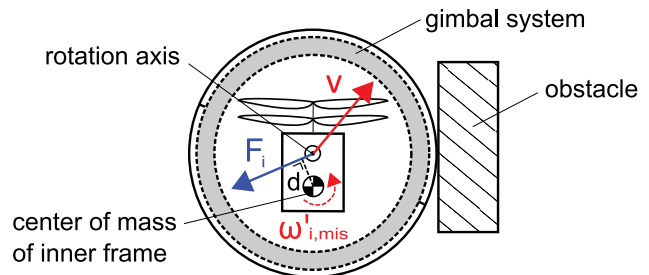
Figure 4. Illustration of the disturbance provoked by an impact when the COM of the inner frame is misaligned with respect to the rotational axis. When a collision occurs, the impact force is transmitted to the inner frame through the axes of the gimbal system, the resultant force $\mathbf{F}_i$ being applied at the crossing of each rotational axis of the gimbal system. Because of inertia, the inner frame will rotate when the impact occurs, which can be avoided by minimizing the lever arm d.

the gimbal system's rotation axes, which generates a lever arm d and thus a torque on the COM. To get a sense of the order of magnitude of the disturbance, the angular speed resulting from a collision of a misaligned inner frame is studied.

For simplifying purposes, we assume here a frontal collision ($v_x = 0$) and thus $\mathbf{F}_i = \mathbf{F}_y$. The angular speed $\omega'_{i,\mathrm{mis}}$ just after the impact resulting from the force $\mathbf{F}_i$ being applied on the inner frame whose COM is misaligned can be obtained using the conservation of momentum:

$$\omega'_{i,\mathrm{mis}} = \frac{F_i d \Delta t}{I_i} = \frac{m_i v d}{I_i}(e_y + 1), \tag{8}$$

where I_i is the moment of inertia of the inner frame and d is the lever arm. $\omega'_{i,\text{mis}}$ can be compared to the spin provoked by a perfectly sideways collision ($v_y = 0$) on a conventional platform not equipped with a gimbal system [from Eq. (3)]:

$$\omega' = \frac{mvr}{I + mr^2}(e_x + 1). \qquad (9)$$

Assuming similar tangential and perpendicular COR ($e_x \approx e_y$), it can be seen that if the misalignment is

$$d_0 = r\,\frac{I_i}{m_i}\,\frac{m}{I + mr^2}, \qquad (10)$$

the disturbance generated by the misaligned gimbal system may be equivalent to the disturbance it aims at removing. Equation (10) can be used when designing a platform to set tolerances on the balancing of the inner frame, which should be at least an order of magnitude below d_0 for the gimbal system to bring a significant advantage.

The COM of the inner frame has to be aligned with each rotation axis, which means that the three rotation axes of the gimbal system have to intersect in one point. While they have a lower mass and moment of inertia, the two moving gimbals should also be balanced for the same reason described above.

After an impact, the outer frame rotates at an angular speed defined by Eq. (3), with a rotation axis perpendicular to the collision plane. The rotation of the outer frame lasts until the friction brings it to a stop. However, if the COM of the outer frame is misaligned with respect to the crossing of the gimbal system's axes, the rotation of the outer frame will generate a centrifugal force that may generate unnecessary disturbances on the inner frame. This type of disturbance can thus be minimized by keeping the COM of the outer frame close to the crossing of the gimbal system's rotational axes.

4. A COLLISION-RESILIENT FLYING ROBOT

To validate the concept presented in the previous section, a prototype, named GimBall, has been designed and built. This section presents the most important aspects of the mechanical design, which implement the guidelines stated in Section 3. The embedded sensors that allow the robot to be fully autonomous are then presented. The prototype of the GimBall robot and its main components are shown in Figure 5.

4.1. Protective Structure

The outer frame should prevent external objects from touching the inner frame or the gimbal system and should not strongly affect the propulsion system, typically by obstructing the airflow. In addition, while remaining lightweight, the outer frame should be able to absorb collision energy without breaking, and should be stiff enough to protect the

gimbal system and inner frame. A spherical polyhedron-shaped protective frame was chosen, as it facilitates rolling on obstacles, and such a structure is able to absorb a relatively high collision energy for its weight by sharing the load among all the structure. The protective structure is made of pultruded carbon fiber rods fixed to each other by 3D-printed acrylonitrile butadiene styrene (ABS) connecting parts and arranged so that each beam defines an edge of a polyhedron of radius $r = 17$ cm. The numerous beams prevent most external objects from touching the gimbal system or the inner frame, and they have a relatively low aerodynamic impact because of their small diameter. We did not perform exhaustive crash tests with this protective cage, but it survived numerous collisions at speeds up to 3 m/s (which corresponds to a free-fall from about 50 cm). Collisions at higher speeds led to the failure of some 3D-printed parts of the protective frame or the gimbal system's joints. To reduce the risks of a gimbal lock and a subsequent loss of degree of freedom, the COM of the protective frame is slightly misaligned with respect to the rotational axes so as to favor an orientation away from a gimbal lock. This misalignment is kept low in order to limit the centrifugal forces generated by the rotation of the protective frame.

4.2. Gimbal System

Lightweight half rings made of carbon fiber sandwiches were manufactured in-house and are held in place by 3D-printed parts. To minimize friction in the joints even when high loads are applied (e.g., during collisions), ball bearings are used for the rotational joints. The design minimizes the distance between the gimbals in order to reduce the size and mass of the whole system. The gimbals are symmetric so that they are balanced with respect to their rotation axis. The assembly of the gimbals is performed carefully so that each pair of rotational joints is aligned with each other and so that the three rotational axes of the system intersect in a center point.

4.3. Inner Frame

The platform must be capable of hover and slow lateral flight in order to be maneuverable in cluttered environments, and thus a VTOL (vertical takeoff and landing) configuration has to be selected [e.g., multirotor platforms (Bristeau et al., 2011; Kalantari and Spenko, 2013), helicopters, coaxial platforms with fly-bar (Dees and Yan, 2012), or control surfaces (Klaptocz, 2012)]. To keep the size and mass of the protective structure low, the propulsion system with the highest lift per area is chosen. A coaxial configuration is thus selected as it provides a good lift-to-area ratio and the two propellers make the best use of the round area offered by the gimbal system. The motor is a CR2805 Himax Contra-Rotating motor. Control surfaces actuated by servomotors
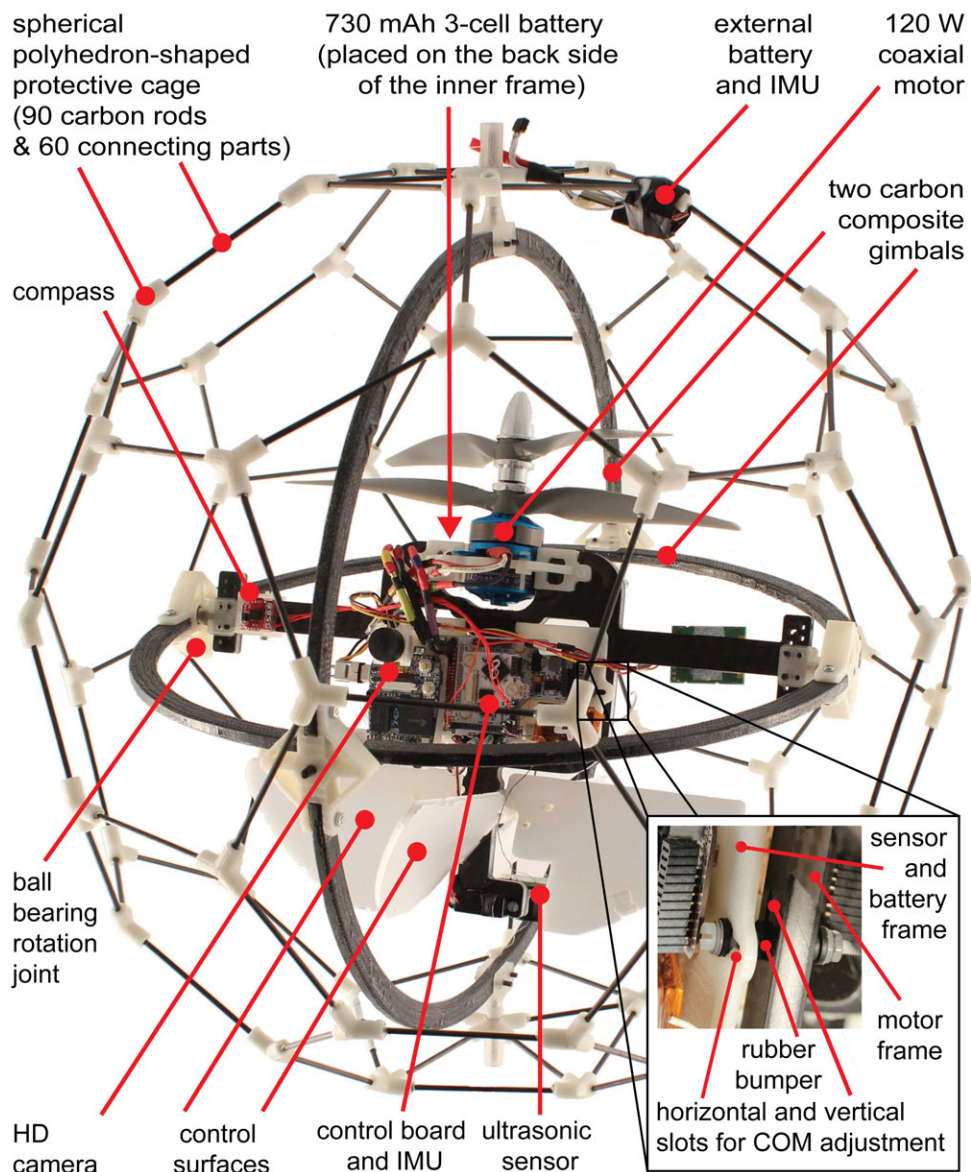
Figure 5. Prototype of a collision-resilient flying robot. A gimbal system allows the protective frame to rotate independently from the inner frame, thus preventing the orientation of the inner frame from being disturbed by collisions. The inner frame is comprised of a coaxial motor for lift, flaps for stabilization, and the avionics that allow the robot to fly fully autonomously. The outer frame is in the shape of a spherical polyhedron, which also enables the platform to roll on obstacles.

are used for controlling the roll and pitch of the platform, while the yaw is controlled by the differential actuation of the coaxial motors.

The inner frame is designed to have its COM at the crossing point of the three rotational axes of the gimbal system. For this purpose, the inner frame comprises two subframes whose positions can be changed thanks to elongated slots so that the COM can be precisely adjusted (inset of Figure 5). The first subframe is the motor frame and is made of carbon fiber sandwich. The second subframe is the electronics frame and is placed in the central part of the motor frame. It is made of a 3D-printed ABS part on which the battery, the high-definition (HD) camera, and the electronic boards are fixed. This frame is isolated from the motor frame by rubber dampers, so as to reduce the noise on the sensors from motor vibrations.

4.4. Sensors and Control Electronics

The embedded sensors and electronics allow for autonomous attitude stabilization of the inner frame as well as altitude and magnetic heading control. Two dsPic33 onboard processors are used for sensor reading, signal processing, and motor control. A six-axis IMU comprised of an ITG 3200 gyroscope and MMA7455L accelerometer and an HMC5843 three-axis magnetometer are used together with a Kalman filter to measure the attitude of the inner frame and the yaw angle with respect to magnetic north. The gyroscope has a $\pm 2,000°$/s range and the accelerometer has a ± 80 m/s^2 range. The fast sampling rate of the gyroscope (500 Hz in this case) allows the robot to keep a correct attitude estimate even after a collision. Indeed, the high temporal resolution keeps the angular rate integration precise even in case of quick changes of angular speed. At the bottom of the inner frame, an ultrasonic sensor is mounted pointing downward to measure the altitude of the robot. Since the altitude measurements are very noisy, especially because the ultrasonic sensor's field of view is frequently obstructed by elements of the protective frame, a Kalman filter is used to fuse the altitude measurements with the vertical acceleration measured by the accelerometers.

Proportional-integral-derivative (PID) controllers are used to control the four degrees of freedom of the robot, that is to say the yaw, pitch, roll, and thrust. While the attitude estimation filter runs at 50 Hz, the derivative command of the PID controllers is updated at 500 Hz to ensure a fast reaction to orientation disturbances. To fly toward a desired direction, a nonzero command for the pitch or roll angles is set by the controller, which provokes a lateral motion of the platform. However, this way of controlling a direction of travel is relatively imprecise, as there is no feedback loop correcting for constant directional errors that could be provoked by a slight imbalance of the platform or the aerodynamic drag.

An additional inertial measurement unit (IMU) and battery are placed on the protective frame to record parameters such as angular velocity in order to characterize the effect of collisions. An 808 HD Micro Camera recording HD video on a microSD card is mounted on the inner frame for demonstration purposes.

4.5. Weight Distribution

The total weight of the prototype is 385 g. Table I gives an overview of the weight of the different components present on the platform, as well as the moments of inertia of the inner frame I_i and of the protective structure I_p (including the gimbal system). It can be seen that the inner frame makes up two-thirds of the total weight of the robot. The cost for having a collision-resilient platform is thus a third of the total weight, corresponding to the gimbal system and protective frame. The inner frame, however, accounts for less than half of the total moment of inertia of the platform,

Table I. Weight distribution for the GimBall platform.

	Weight (g)	Moment of inertia (kg cm^2)
Protective structure	**84**	$I_p = 17.9$
Gimbal system	**56**	
Inner frame	**245**	$I_i = 13.7$
coaxial motor	59	
battery	57	
electronics	22	
camera	7	
motor frame, servos, flaps, other parts	100	
Total	**385 g**	$I = 31.6$

which suggests that the attitude control of the inner frame can be two times faster than if it had been rigidly attached to the protective structure.

Using the numbers from Table I, we can compute d_0 using Eq. (10):

$$d_0 = 0.17 \frac{1.37 \times 10^{-3}}{0.245} \frac{0.385}{(3.16 \times 10^{-3}) + (0.385 \times 0.17^2)}$$

$$= 2.6 \text{ cm}, \tag{11}$$

which means that if the COM of the inner frame has an offset with respect to the axes of rotation in the order of 2.6 cm, the disturbance from a collision may be as big with the gimbal system as without the gimbal system. This number gives a good idea of the precision with which the COM should be aligned with the axes of rotation in order to ensure a proper reduction of the disturbances. A good target would typically be a COM alignment precision of at least $d_0/10 = 2.6$ mm.

5. EXPERIMENTS

To validate the concept presented in Section 3 and the viability of the prototype presented in Section 4, the performance of the prototype at reducing disturbances is first tested thanks to repeatable collision experiments. To characterize the performance, an extension of the collision model presented in Section 2 is introduced to account for the two independently rotating frames of the prototype. The prototype is tested in the field in remote-controlled mode and in autonomous mode. A simple navigation algorithm is implemented as a proof-of-concept to demonstrate how the robot can fly in cluttered environments without the need for complex sense and avoid techniques.

5.1. Extended Collision Model

Because the inner frame and protective frame of the prototype rotate independently, we propose using two tangential coefficients of restitution e_x to characterize both
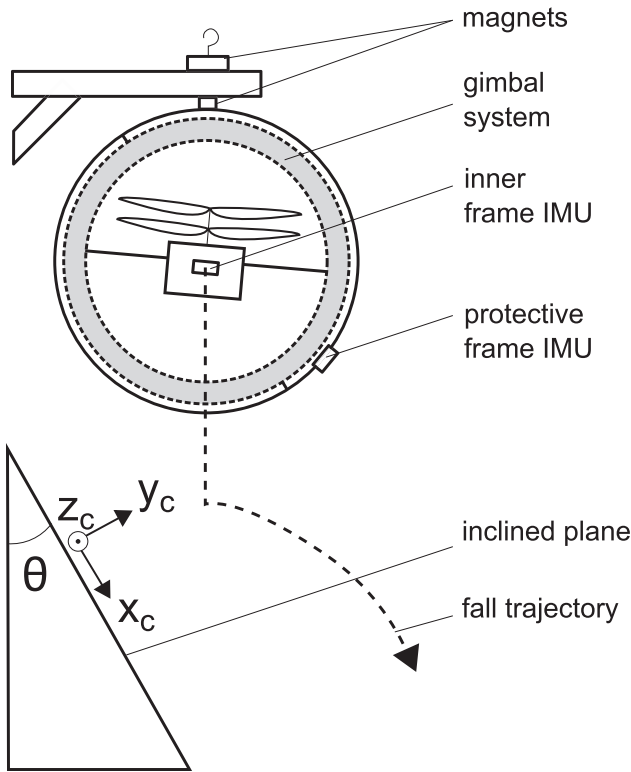
Figure 6. Experimental setup used to determine the tangential COR of the protective frame and the inner frame, allowing characterization of the performance of the gimbal system at reducing disturbances provoked by the frictional force during an impact. A 1-mm-thick linoleum sheet was placed on the plane to increase friction.

frames' reactions to the friction force. In the case of a conventional platform whose protective frame is rigidly attached to the central body, the tangential COR can be obtained by measuring v_x and ω', assuming that I, m, and r are known, thanks to Eq. (3):

$$e_x = -1 + \frac{r\omega'(\alpha + 1)}{v_x}. \tag{12}$$

To extend the model described by Eqs. (1)–(7) to a platform whose inner frame and protective frame rotate independently after an impact at angular speeds ω'_i and ω'_p, respectively, we propose defining two tangential CORs for the inner frame and protective frame as follows:

$$e_{x,i} = -1 + \frac{r\omega'_i(\alpha_i + 1)}{v_x}, \tag{13}$$

$$e_{x,p} = -1 + \frac{r\omega'_p(\alpha_p + 1)}{v_x}, \tag{14}$$

where $\alpha_i = \frac{I_i}{m_i r^2}$ and $\alpha_p = \frac{I_p}{m_p r^2}$, where I_i is the moment of inertia of the inner frame, m_i is the mass of the inner frame,
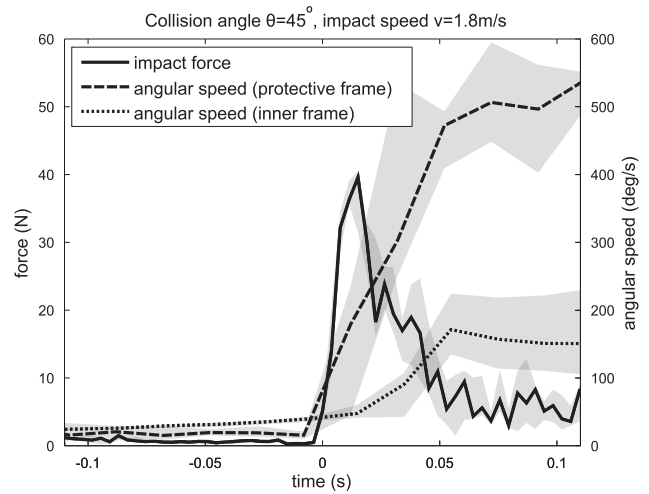
Figure 7. Example of impact force and angular rates recorded during multiple collisions on an inclined plane thanks to the IMUs mounted on each frame. The shaded areas show the interquartile range (seven trials total). The impact starts at $t = 0$ and lasts approximately 50 ms. It can be observed that, as expected, the protective frame rotates faster after the impact than the inner frame. Such experiments are repeated for 16 different collision types (with different speeds, angles, or platform types).

I_p is the moment of inertia of the protective frame, m_p is the mass of the protective frame, and r is the distance between the point of impact and the COM, assuming identical positions of both the inner and protective frames' centers of mass. As in the original model, the COR describes the sensitivity of each frame to friction during a collision.

5.2. Collision Experiments

The collision experiments are aimed at characterizing how the orientation of the inner frame is affected by collisions, so the inner frame's COR $e_{x,i}$ is of particular interest. Ideally, $\omega'_i = 0$ and $e_{x,i} = -1$, which corresponds to a virtually frictionless collision "as seen" by the inner frame (even though there may have been friction between the protective frame and the obstacle). However, mechanical imperfections may result in an imperfect decoupling between the inner frame and the protective frame, which is reflected in a tangential COR higher than -1.

To measure the effectiveness of the prototype presented in Section 4 at reducing disturbances, the test setup described in Figure 6 is used. Taking inspiration from the experiments performed by Cross (2002), the prototype is dropped at multiple speeds (1 and 1.8 m/s, which corresponds to typical flight speeds) on planes inclined at different angles ($\theta = 15°$, $30°$, $45°$, and $60°$). The prototype is held still before being dropped at zero initial speed thanks to a magnet fixed on the protective frame and a magnet
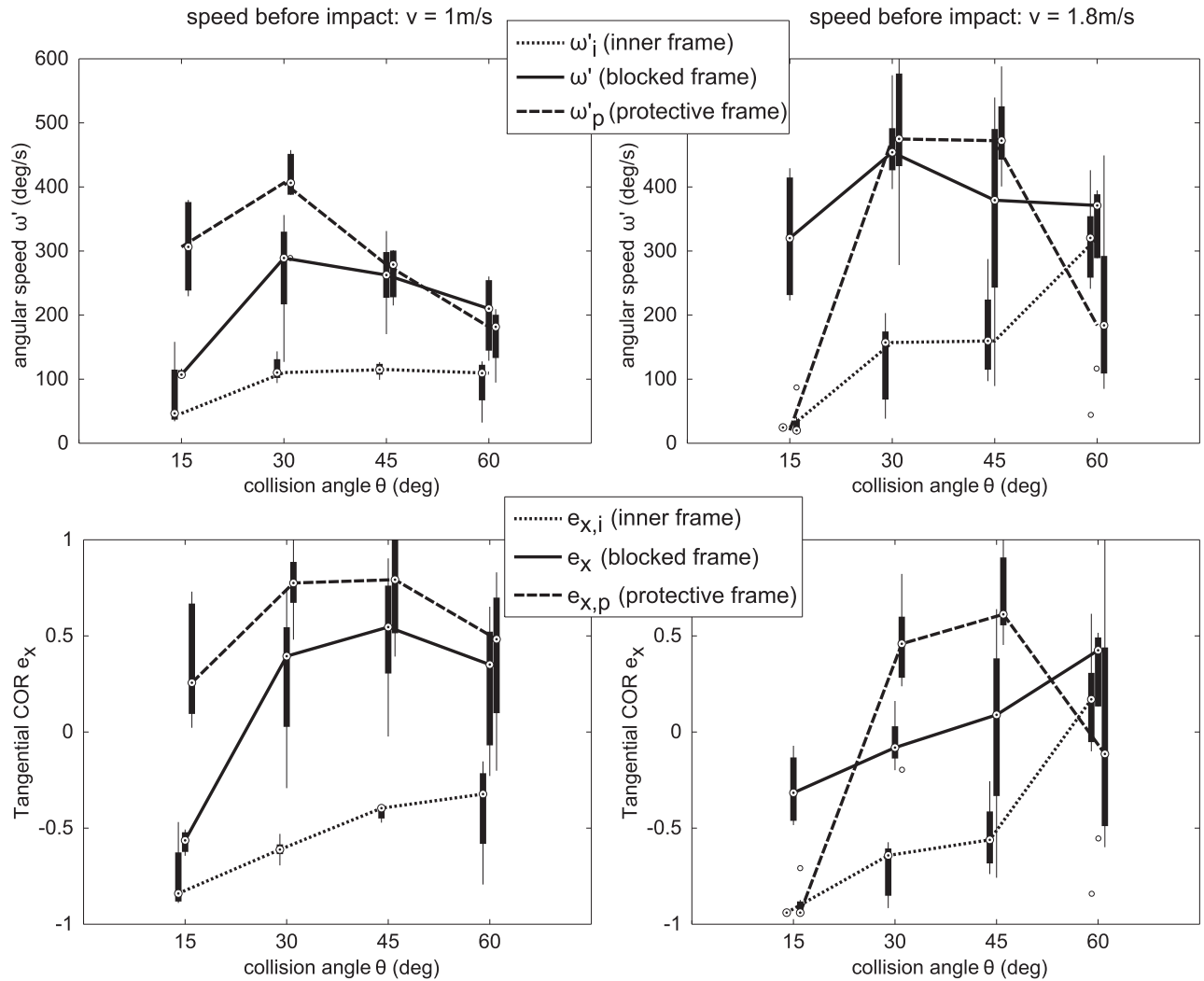
Figure 8. Box plots of the angular speeds and tangential COR of the inner frame, protective frame, and blocked frame measured during multiple collision experiments (speed before impact $v = 1$ and 1.8 m/s, and collision angles $\theta = 15°, 30°, 45°,$ and $60°$). Lower values for the tangential COR mean that the frame is less disturbed by the collision. The values for the inner frame and protective frames are obtained during the same sets of experiments, while the values for the blocked frame are obtained during additional experiments in which the gimbal system was blocked.

above a supporting beam, which is removed to initiate the drop. IMUs fixed to the inner frame and protective frame record accelerations, angular speeds, and orientation at high frequency. Parameters such as the angular speed after the impact, the speed before the impact, or the contact force amplitude and direction can be measured.

The experiments are performed with a freely rotating gimbal system and with a blocked gimbal system preventing any rotation (referred below as a "blocked frame"). Blocking the gimbal system emulates existing caged platforms with equivalent shape and mechanical properties (mass, moment of inertia, elasticity, coefficient of friction,

etc.). Two IMUs record the acceleration vector at 267 Hz and the angular speed vector at 50 Hz and provide the orientation of each frame. The acceleration and angular speed vectors are converted in the inertial frame of reference aligned with the collision plane (X_c; Y_c; Z_c). The accelerometers precisely measure the free-fall time Δt_{ff} (during which they measure zero acceleration), and the speed before the impact v can thus be obtained assuming no aerodynamic drag. Finally, acceleration measurements are multiplied by the robot's mass to obtain the impact force.

Between five and ten collisions are recorded for each collision type. The inner frame is positioned in a random

starting orientation, making sure that the gimbals are not in a gimbal-lock situation. A MATLAB script automatically detects the beginning and end of the collision and processes the data. Typically, the angular speeds just after the impact are used to compute the tangential COR thanks to Eqs. (13) and (14). The values for I, m, I_i, m_i, I_p, and m_p are taken from Table I, with the gimbal system accounting for the weight and moment of inertia of the protective frame, and assuming that the moment of inertia is approximately constant in all directions. As an example, measurements obtained for a typical experiment (seven collisions at angle $\theta = 45°$ and $v = 1.8$ m/s) are shown in Figure 7.

The tangential COR of the inner frame is significantly lower than for the blocked frame in most cases, except for $\theta = 15°$ at $v = 1.8$ m/s, where both COR correspond to frictionless contacts, and $\theta = 60°$ at $v = 1.8$ m/s (Figure 8). Therefore, the gimbal system succeeds at reducing the disturbance from contacts during these experiments, except for the case in which $\theta = 60°$ and $v = 1.8$ m/s. However, the tangential COR of the inner frame is in all cases significantly higher than -1, the ideal value, except for $\theta = 15°$ at $v = 1.8$ m/s. Although these experiments validate the gimbal system concept for inner frame stabilization after collisions, they also raise interrogations about the cause of the remaining disturbances on the inner frame.

It can be seen that the COR of the inner frame is not constant across all collision types, which means that the gimbal system is more effective in certain cases than others at reducing disturbances. A trend seems to indicate that higher collision angles increase the COR $e_{x,i}$ of the inner frame (bottom graphs of Figure 8), indicating lower performance. Typically, based on Eq. (3) and assuming constant e_x, one could expect the angular speed after the impact ω'_i to decrease when the collision angle increases, but this is not the case (top graphs of Figure 8). A suspected source of perturbation that would explain this is the elasticity of the gimbal system.

This hypothesis is backed by observations of videos obtained with a high-speed camera and further analysis of the contact force during a collision. It is observed that high deformations of the gimbal system (in the order of centimeters) occur during collisions. Furthermore, Figure 9(a) shows that the contact force applied on the platform during a collision changes direction over time. Figures 9(b) and 9(c) show how the combination of these two effects causes a disturbance on the inner frame that increases if the impact force increases. These observations could explain why the disturbances increase with higher impact collision angles, because these correspond to higher impact forces (which reach a maximum in the case in which $\theta = 60°$ and $v = 1.8$ m/s).

To reduce these disturbances and improve the performance of the gimbal system, a guideline for future versions is to maximize the mechanical rigidity of the gimbal system and inner frame. A second suggestion is to design the pro-
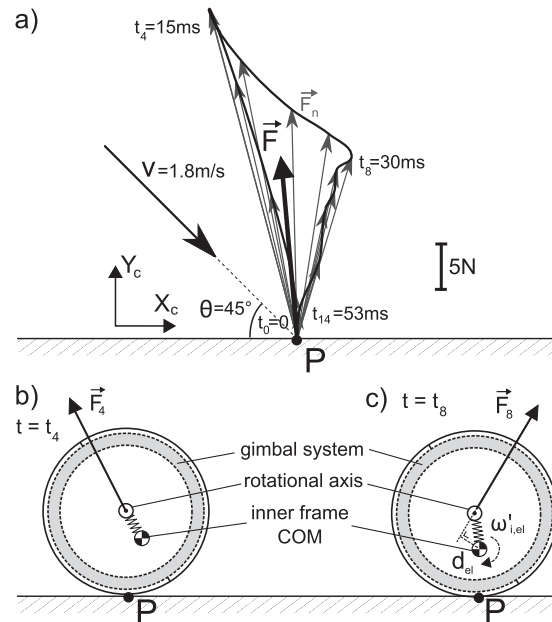

Figure 9. Part (a) shows the evolution over time of the contact force occurring during typical collisions. The profile is obtained by averaging and smoothing inertial data collected during seven collisions with initial speed 1.8 m/s and collision angle $\theta = 45°$. The average force **F** is the result of each instantaneous force $\mathbf{F}_n$ applied at each time step. It can be seen that the direction of the contact force is not constant over the length of the contact. If the gimbal system is not perfectly rigid, but rather acts as a flexible link (or spring), the COM of the inner frame will not remain aligned with the rotation axis during a collision, as shown exaggeratedly in (b). Because of this and the varying force profile, a lever arm d_{el} appears, as shown in (c), and provokes an angular speed $\omega'_{i,el}$ disturbing the inner frame.

tective frame to be relatively elastic so as to reduce the impact force and thus the gimbal system deformation. Finally, another way of limiting the impact force is by controlling the flight speed of the robot so that it remains within a safe threshold.

5.3. Field Tests

Field tests are carried out in a 100-m-long forest, which provides a challenging cluttered environment with uneven obstacles such as trees or branches, and uneven grounds (Figure 10). To show how the gimbal system can reduce the control complexity for navigation at low altitude, a simple autonomous controller is implemented, where the platform is stabilized at constant altitude and given a compass direction to follow. More advanced control strategies could improve the navigation or disturbance reduction, for example by reacting to collision measurements or by adjusting the control parameters during a collision. However, the control

Figure 10. Forest where autonomous flight tests are performed.

aspects are not the focus of this paper, and the experiments are aimed at showing that the collision-resilient flying robot can progress autonomously in a cluttered environment with very simple control.

The flying robot is started at the same position for each trial and given the north direction to follow. The commanded altitude (or height above ground) is 1 m, which is sometimes challenging for the control system to regulate as the ground in the forest is relatively uneven. Additionally, as described in Section 4.4, the altitude estimation may be noisy due to challenging conditions for the sonar sensor. Similarly, the direction followed by the robot cannot be accurately controlled, and thus varies slightly from trial to trial. The travel speed is set around 1.5 m/s, but it varies as well from trial to trial because of the lack of closed-loop control for lateral motions. The trials were stopped either when the flying robot was not able to recover from a collision with an obstacle, or once the robot reached the limits of the experimental area. A hand-held GPS device (Garmin Vista HCx) carried by a human following the robot is used to obtain recordings of the trajectories. Videos are recorded by the internal camera for each trial, and some of these can be seen at the end of the accompanying video.

A total of six trials were performed (Figure 11) during which 24 collisions with obstacles were recorded, which corresponds to four collisions per trial on average. While many obstacles (trees) are vertical, the pitch and roll axes of the protective frame are often disturbed by collisions (Figure 12) because of the multiple altitude corrections that cause the velocity before impact to be off the horizontal plane. While there are still obstacles that can incapacitate the current prototype, especially because they can penetrate inside the protective cage, the experiments successfully demonstrate that the robot can autonomously fly through a forest at relatively high speed.

6. CONCLUSION

This paper describes a concept of collision-resilient flying robots and demonstrates its viability by means of a proof-
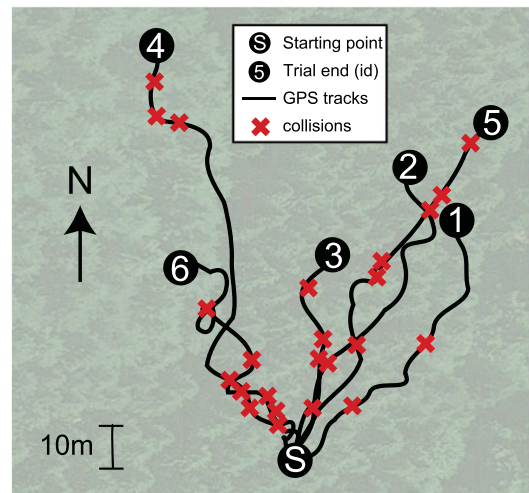

Figure 11. GPS tracks obtained by a human carrying a hand-held GPS device (Garmin Vista HCx) and closely following the robot during the experiments. The flying robot is initialized at the same position for each trial, and is programmed to fly toward the north direction. Red crosses indicate each time a collision with an obstacle occurs (landmarks were recorded manually in the hand-held GPS device when collisions were observed, and the exact timing of the collision was confirmed afterwards thanks to data logs and the onboard video). The robot flew a total distance of 470 m in about 5 min, which corresponds to an average speed of 1.5 m/s. It can be seen from the GPS tracks that the exact direction followed by the robot is not constant from trial to trial, but the robot still goes approximately toward the north, as commanded.

of-concept prototype equipped with a gimbal system that reduces the effects of collisions on the platform's stability. The collision model enabled the formulation of design guidelines, leading to the prototyping of GimBall, a collision-resilient platform. Its performance at reducing the effect of collisions on the inner frame was characterized and assessed in multiple collision experiments and validated in autonomous flights in a dense forest. Furthermore, the
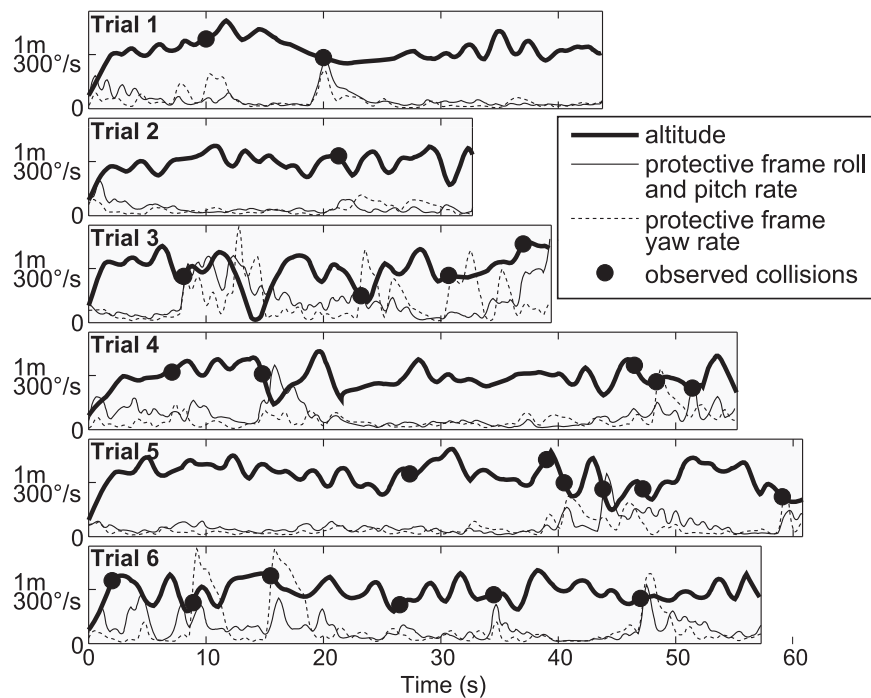
Figure 12. Time series of the altitude and protective frame angular speeds for each trial shown in Figure 11. The robot autonomously maintains its altitude and direction and flies through the forest while experiencing collisions. Trial 1 was stopped because of a collision involving a branch entering in the structure of the robot, and trials 3 and 6 were manually stopped because of a failure of the altitude control to keep the robot at a correct height. Trials 2, 4, and 5 were manually stopped once the robot reached the end of the experiment area. It can be seen that some collisions cause rotations of the protective frame around the roll, pitch, or yaw axes, which diminish after several seconds. The angular rates are expressed in the earth's reference frame.

design allows for takeoff from arbitrary orientations (as shown in the accompanying video) by rotating the inner frame with a small thrust and regulation of the control surfaces in the appropriate direction.

Two major characteristics affecting the capability to stabilize after a collision were highlighted: (a) The center of mass of the inner frame should be carefully aligned with the axes of the gimbal system, and (b) the rigidity of the gimbal system should be maximized while the protective frame should be softened to reduce impact energy. Other characteristics are expected to play an important role as well, such as the friction in the passive rotation joints that should be minimized, or the gimbal lock situation that should be avoided.

Future work will focus on structures to protect the robot from protruding obstacles for increased collision resilience in harsh environments. Methods to detect the collision angle based on the inertial sensors and collision model or additional force sensors will be investigated, enabling more advanced behaviors using collision information for navigation as suggested by Briod et al. (2013). We will also study locomotion strategies involving constant contact with the environment, such as rolling on the ground or against ob-

stacles as suggested by Kalantari and Spenko (2013). We also envision the use of sensors for ego-motion estimation in order to better control the flight direction of the platform, as well as to keep the flight speed under a safe value. All these developments are intended to pave the way toward robust flying robots capable of operating in difficult environments found in search-and-rescue missions.

APPENDIX

The accompanying video[1] (4:39) shows remote-controlled flights in various environments and then the videos recorded with the onboard camera during trials 2, 4, and 5.

REFERENCES

Bachrach, A., He, R., & Roy, N. (2009). Autonomous flight in unknown indoor environments. International Journal of Micro Air Vehicles, 1(4), 217–228.

Briod, A. (2008). Observation of insect collisions. Technical report, Harvard University & EPFL, Boston.

Briod, A., Kornatowski, P., Klaptocz, A., Garnier, A., Pagnamenta, M., Zufferey, J.-C., & Floreano, D. (2013). Contact-based navigation for an autonomous flying robot. In IEEE/RSJ International Conference on Intelligent Robots and Systems.

Bristeau, P., Callou, F., Vissière, D., & Petit, N. (2011). The navigation and control technology inside the ar. drone micro UAV. In 18th IFAC World Congress (pp. 1477–1484).

Cross, R. (2002). Measurements of the horizontal coefficient of restitution for a superball and a tennis ball. American Journal of Physics, 70(5), 482.

Dees, J., & Yan, G. (2012). Self-righting frame and aeronautical vehicle. EP Patent 2,517,767.

Domenech, A. (2005). A classical experiment revisited: The bounce of balls and superballs in three dimensions. American Journal of Physics, 73(1), 28.

Garwin, R. L. (1969). Kinematics of an ultraelastic rough ball. American Journal of Physics, 37.

Itasse, M., Moschetta, J.-M., Ameho, Y., & Carr, R. (2011). Equilibrium transition study for a hybrid MAV. International Journal of Micro Air Vehicles, 3(4), 229–246.

Kalantari, A., & Spenko, M. (2013). Design and experimental validation of HyTAQ, a hybrid terrestrial and aerial quadrotor. In IEEE International Conference on Robotics and Automation (pp. 4430–4435).

Klaptocz, A. (2012). Design of flying robots for collision absorption and self-recovery. Ph.D. thesis, Ecole Polytechnique Fédérale de Lausanne.

Klaptocz, A., Boutinard-Rouelle, G., Briod, A., Zufferey, J.-C., & Floreano, D. (2010). An indoor flying platform with collision robustness and self-recovery. In IEEE International Conference on Robotics and Automation (pp. 3349–3354).

Klaptocz, A., Briod, A., Daler, L., Zufferey, J.-C., & Floreano, D. (2013). Euler spring collision protection for flying robots. In IEEE/RSJ International Conference on Intelligent Robots and Systems.

Klaptocz, A., Daler, L., Briod, A., Zufferey, J.-C., & Floreano, D. (2012). An active uprighting mechanism for flying robots. IEEE Transactions on Robotics, 28(5), 1152–1157.

Kumar, V., & Michael, N. (2012). Opportunities and challenges with autonomous micro aerial vehicles. The International Journal of Robotics Research, 31(11), 1279–1291.

Marconi, L., & Naldi, R. (2012). Control of aerial robots: Hybrid force and position feedback for a ducted fan. IEEE Control Systems, 32(4), 43–65.

Roberts, J. F., Stirling, T. S., Zufferey, J.-C., & Floreano, D. (2007). Quadrotor using minimal sensing for autonomous indoor flight. In European Micro Air Vehicle Conference and Flight Competition (EMAV2007) (pp. 17–21).

Scaramuzza, D., Achtelik, M. C., Doitsidis, L., Fraundorfer, F., Kosmatopoulos, E. B., Martinelli, A., Achtelik, M. W., Chli, M., Chatzichristofis, S. A., Kneip, L., Gurdan, D., Heng, L., Lee, G. H., Lynen, S., Meier, L., Pollefeys, M., Siegwart, R., Stumpf, J. C., Tanskanen, P., Troiani, C., & Weiss, S. (2013). Vision-controlled micro flying robots: From system design to autonomous navigation and mapping in GPS-denied environments. IEEE Robotics & Automation Magazine.

Schafroth, D., Bouabdallah, S., Bermes, C., & Siegwart, R. (2008). From the test benches to the first prototype of the muFly micro helicopter. Journal of Intelligent and Robotic Systems, 54(1-3), 245–260.

Shen, S., Michael, N., & Kumar, V. (2011). Autonomous multi-floor indoor navigation with a computationally constrained MAV. In Robotics and Automation (ICRA), 2011 IEEE International Conference (pp. 20–25). IEEE.

Spletzer, B. L., Fischer, G. J., & Martinez, M. A. (2001). Passive orientation apparatus. U.S. Patent 6,286,386.

Zufferey, J.-C., Beyeler, A., & Floreano, D. (2009). Optic flow to steer and avoid collisions in 3D. Flying Insects and Robots (pp. 73–86).

---

[1]https://documents.epfl.ch/groups/l/li/lis-unit/www/Research/GimBall/GimBall.mp4